Elastic and Inelastic Scattering of Protons by Carbon-12 for Proton Energies between 18 and 30 MeV*†

J. KIRK DICKENS,‡ DAVID A. HANER, AND CHARLES N. WADDELL
University of Southern California, Los Angeles, California
(Received 8 July 1963)

Differential cross sections for elastic scattering of protons by C^{12} have been measured for incident proton energies between 18 and 30 MeV. Angular distributions were obtained for proton energies of 20.0, 21.6, 24.1, 26.1, and 27.8 MeV. The elastic differential cross section as a function of energy for center-of-mass angles of 46.7°, 60.6°, 135.0°, and 145.0° was investigated for incident energies between 17.6 and 30.4 MeV. Absolute angular distributions and integrated partial cross sections for proton scattering leading to the excitation of the 4.4-, 7.7-, 9.6-, and 12.7-MeV levels in C^{12} are reported. The angular distributions of the elastically scattered protons are strongly energy-dependent over the studied energy interval. The inelastic angular distributions do not exhibit such a marked energy dependence and are peaked forward for all levels studied. The angular distributions of protons inelastically scattered from the 4.4-MeV level are compared with the predictions of the zero-range, plane-wave Born-approximation direct-interaction theory.

I. INTRODUCTION

RECENT optical-model analysis of the elastic scattering of 12- to 19-MeV protons by carbon indicates that excellent fits to the experimental data can be obtained using a potential characterized primarily by a thin absorptive shell.[1] As the first step in an experimental program to extend the measurements of elastic scattering of protons by carbon to the 20- to 30-MeV range, the results at 31.1 MeV were obtained and analyzed.[2] The optical-model parameters obtained at 31 MeV, in particular those corresponding to the absorptive potential, indicate a definite change from those obtained for $E_p \leqslant 19$ MeV. At 31 MeV it is necessary to include volume absorption. This unmistakable change encouraged the continuation of the experimental program; angular distributions of protons elastically scattered by carbon at five energies between 20 and 28 MeV are presented in this paper.

The angular distributions of protons inelastically scattered from several excited states[3] of C^{12} were also obtained and are presented. These differential cross sections are peaked forward and are not symmetric about 90°, and vary slowly with incident proton energy, as do those reported for 14 MeV $\leqslant E_p \leqslant$ 19 MeV.[4]

II. EXPERIMENTAL DETAILS

A. General

The equipment in the bombardment area is shown in Fig. 1. Protons, after acceleration in the University of Southern California proton linear accelerator to 31.5 MeV, were reduced in energy by an absorber, collimated by nickel collimators, allowed to strike a target, and collected in a Faraday cup. Except for the incident-beam energy degradation by an absorber, the experimental procedure has been described in detail.[2] A resumé of this procedure is presented here.

The general purpose scattering stand included a vacuum target chamber, provided precise determination of geometrical parameters, and supported adequate shielding for the counter assembly. The protons scattered by the polystyrene (CH) target were detected by a counter telescope consisting of a gas proportional counter and a $\frac{1}{4}$-in. thick NaI(Tl) scintillation counter. Pulses from the NaI crystal coincident with appropriate pulses from the proportional counter were analyzed by a multichannel pulse-height analyzer. Counting losses in the pulse-height analyzer were monitored during each run, and these losses were kept below 5% by maintaining a moderate counting rate. The proton beam was stopped in a carbon Faraday cup. The collected charge was integrated using a calibrated low-leakage polyethylene capacitor and the emf was measured with a 100% feedback electrometer.

B. Beam Energy Reduction

The energy of the beam from the linear accelerator cannot be changed appreciably by varying machine parameters[5]; therefore, it was necessary to use an absorber to reduce the energy of the beam. Two absorbing materials, aluminum and hydrogen, were used.

Aluminum was chosen initially as the absorbing material and was used during the runs at 20.0 and 27.8 MeV. However, the beam intensity of the reduced energy beam was much less than that obtained at full beam energy due to multiple scattering. Another difficulty encountered, especially at 20 MeV, was the in-

* Work supported in part by the U. S. Atomic Energy Commission.
† Part of a thesis submitted by JKD to the Faculty of the Graduate School, University of Southern California in partial fulfillment of the requirements for the Ph.D. (Physics) degree.
‡ Present address: Oak Ridge National Laboratory, Oak Ridge, Tennessee.
[1] J. S. Nodvik, C. B. Duke, and M. A. Melkanoff, Phys. Rev. **125**, 975 (1962).
[2] J. K. Dickens, D. A. Haner, and C. N. Waddell, Phys. Rev. **129**, 743 (1963).
[3] F. Ajzenberg-Selove and T. Lauritsen, Nucl. Phys. **11**, 1 (1959).
[4] R. W. Peelle, Phys. Rev. **105**, 1311 (1957).
[5] L. W. Alvarez, H. Bradner, J. V. Franck, H. Gordon, J. D. Gow, L. C. Marshall, F. Oppenheimer, W. K. H. Panofsky, C. Richman, and J. R. Woodyard, Rev. Sci. Instr. **26**, 111 (1955).

tense low-energy background from neutrons produced in the absorber. These considerations prompted an investigation of other absorbing materials, and hydrogen gas was used for the remainder of the study.

The hydrogen gas, contained in the last 13 ft of the beam pipe, was separated from the vacuum of the linear accelerator by a 0.005-in. aluminum foil (see Fig. 1). Gas contained at pressures up to 100 psi could reduce the beam energy down to 17.5 MeV. Using hydrogen gas instead of aluminum as an absorber increased the beam intensity and greatly reduced the background. Spread in the incident beam was about 300 keV at full-beam energy.[5] At 20 MeV, with an aluminum absorber, this spread was observed to be about 800 keV. At 17.6 MeV, with the hydrogen absorber, this spread was observed to be about 450 keV.

The incident beam energy was determined by calculating the energy loss[6] of the protons in the degrading system and subtracting this from the full-beam energy. Methods of energy determination used as checks were (a) comparing the pulse heights of elastically scattered protons before and after beam-energy reduction, (b) measuring the proton-proton cross section at 45° laboratory angle and comparing this measurement with previously determined values,[7] and (c) measuring elastic differential cross sections for proton-C^{12} scattering at energies <19.4 MeV and comparing these with the data of R. W. Peelle[4] and W. Daehnick and R. Sherr.[8]

The beam energies for the five fixed-energy sets of differential cross sections are presented in Table I. Quoted errors indicate the estimated reliability of the beam-energy determination.

III. EXPERIMENTAL RESULTS

A. Observed Spectra

Data were taken at 3- to 10-deg intervals between the laboratory angles of 10 and 156 deg. The laboratory angles were usually chosen to give integral center-of-mass angles for the elastic peak.

Figure 2 shows pulse-height spectra from the scintillation counter obtained at 21.6 and 27.8 MeV. The peaks corresponding to protons scattered by the ground state and the first three excited states are clearly distinguished. However, as the figure shows, the peaks corresponding to protons scattered by the 7.7- and 9.6-MeV levels are superimposed on a continuum of protons from the reaction, $C^{12}(p,p')3\alpha$, that has a Q value of -7.2 MeV.[3,9]

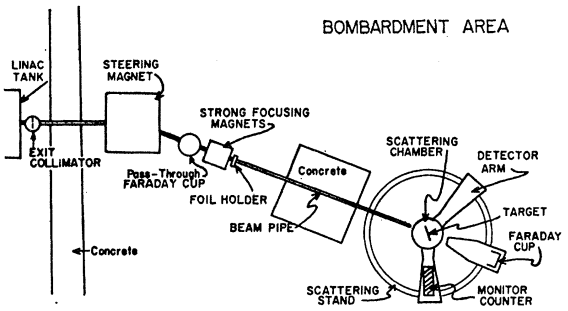

FIG. 1. The experimental arrangement for proton scattering experiments.

B. Reduction of Data

The procedure for data reduction was the same as used at 31 MeV,[2] and features specific to the present experiment are discussed below.

TABLE I. Beam energies.

Run	Mean beam energy[a] (MeV)
1	20.0±0.3[b]
2	27.8±0.1[b]
3	24.1±0.2[c]
4	26.1±0.1[c]
5	21.6±0.1[c]

[a] All of these energies were corrected for energy losses in the following: the foil at the end of the beam pipe, the air between the beam pipe and the scattering chamber, the mylar window on the scattering chamber, and the target thickness.
[b] Using the aluminum degrader.
[c] Using the hydrogen gas degrader.

Three corrections were applied to the yield recorded by the pulse-height analyzer. These were (a) the contribution to the yield from collimator penetration,[10] (b) the effect due to nuclear interactions of the protons entering the NaI crystal,[11] and (c) the correction for counting losses in the pulse-height analyzer. For scattering by the 7.7- and 9.6-MeV levels, the number of protons in the continuum had to be estimated to obtain the net number of counts in a peak. After the total number of counts and estimated subtraction counts were obtained, calculation of each cross section and associated relative and absolute errors in laboratory and center-of-mass coordinates was performed using the University of Southern California Honeywell 800 computer.

IV. RESULTS AND DISCUSSION

A. Elastic Scattering

The measured elastic differential cross sections and associated errors are presented in Table II. Figure 3

[6] W. A. Aron, B. G. Hoffman, and F. C. Williams, University of California Radiation Laboratory Report UCRL-121, 2nd Rev., 1949 (unpublished).
[7] B. Cork, Phys. Rev. **80**, 321 (1952). J. L. Yntema and M. G. White, *ibid.* **95**, 1226 (1954). L. H. Johnston and Y. S. Tsai, *ibid* **115**, 1293 (1959). L. H. Johnstcn and D. E. Young, *ibid.* **116**, 989 (1959). T. H. Jeong, L. H. Johnston, D. E. Young, and C. N. Waddell, *ibid.* **118**, 1080 (1960).
[8] W. Daehnick and R. Sherr (private communication from C. B. Duke).
[9] H. B. Knowles, University of California Radiation Laboratory Report UCRL-3753, 1957 (unpublished). S. S. Vasilyev, V. V. Komarov, and A. M. Popova, Nucl. Phys. **40**, 443 (1963).
[10] E. J. Burge and D. A. Smith, Rev. Sci. Instr. **33**, 1371 (1962).
[11] L. H. Johnston and D. A. Swenson, Phys. Rev. **111**, 212 (1958).

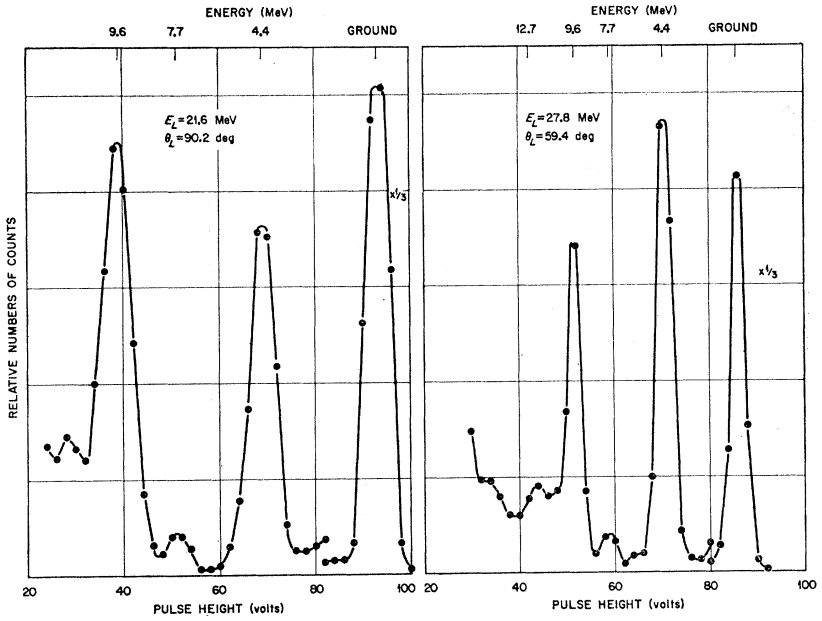

FIG. 2. Scintillation counter coincidence-gated spectrum obtained at 59.4° for $E_p=27.8$ MeV and at 90.2° for $E_p=21.6$ MeV. The peaks corresponding to protons scattered from known levels in C^{12} are indicated.

is a comparison of these results and the data at 31.1 MeV,[2] and emphasizes the variation of angular distribution as the incident proton energy is changed.

This large variation of small cross sections at backward angles caused some concern, since it suggested that some unaccounted for error may have been associated with these measurements. Using the hydrogen gas degradation system, the incident beam energy could readily be changed in small increments permitting study of the elastic differential cross section as a function of energy for several center-of-mass angles. The counter telescope was used to obtain absolute differential cross sections at $\theta_{c.m.}=135°$ and 145°. Simultaneously the monitor counter was used to obtain relative differential cross sections at $\theta_{c.m.}=46.7°$ and 60.6°. The output of this counter was fed into a scaler, with the discriminator set to record only elastically scattered protons.

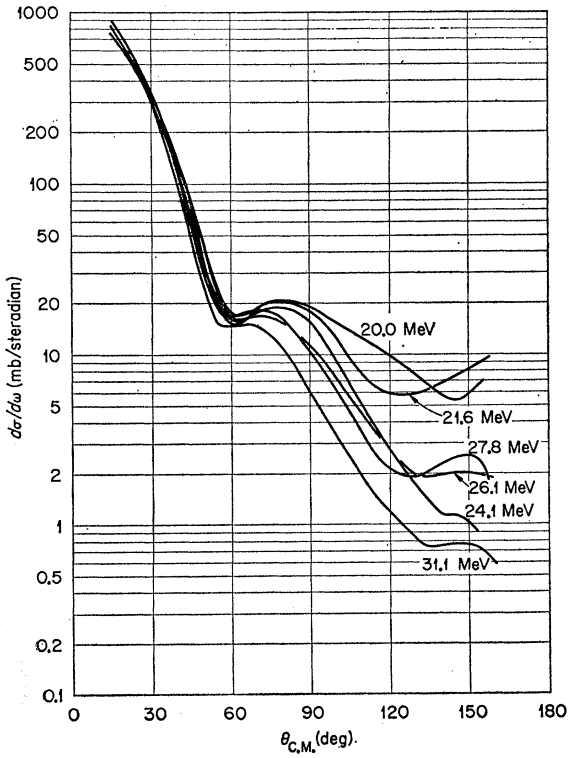

FIG. 3. Elastic scattering angular distributions for 6 energies. The 31.1-MeV curve was taken from Ref. 2.

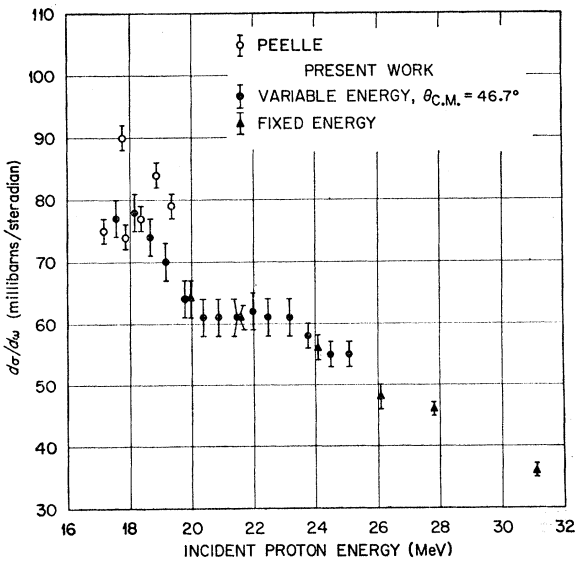

FIG. 4. Differential elastic scattering cross sections at $\theta_{c.m.}=46.7°$. The data labeled "Peelle" were taken from Ref. 4.

TABLE II. Differential cross sections for the elastic scattering of protons by C^{12}.

θ_{lab} (deg)	$(d\sigma/d\omega)_{lab}$ (mb/sr)	$\theta_{c.m.}$ (deg)	$(d\sigma/d\omega)_{c.m.}$ (mb/sr)		Relative % error	Absolute % error
		$E_{lab}=20.0\pm0.3$ MeV				
13.9	982	15.0	841	±41	4.9	6.2
18.5	745	20.0	639	30	4.6	6.1
27.8	396	30.0	343	12	3.5	5.3
32.4	262	35.0	229	8	3.4	5.2
36.9	163	39.8	143	6	4.0	5.7
41.7	93.2	44.9	82.6	2.5	3.0	4.6
46.5	47.4	50.0	42.5	1.6	3.8	5.1
51.1	26.1	54.8	23.6	0.9	4.0	5.2
56.0	18.0	60.0	16.5	0.7	4.3	5.5
58.9	17.4	63.0	16.0	0.7	4.3	5.5
62.8	17.9	67.2	16.7	0.6	3.3	4.8
65.6	20.0	70.1	18.8	0.8	4.1	5.3
70.5	21.8	75.0	20.7	0.8	4.1	5.3
75.4	21.1	80.0	20.3	0.8	4.1	5.3
85.0	19.6	89.8	19.4	0.8	4.0	5.2
93.0	15.8	97.8	16.0	0.6	4.0	5.2
100.6	13.09	105.3	13.55	0.40	3.0	4.1
110.5	10.84	115.0	11.54	0.57	4.9	6.0
120.0	7.91	124.2	8.64	0.34	3.9	5.2
127.1	6.53	130.9	7.26	0.28	3.8	5.1
133.0	5.52	136.5	6.23	0.27	4.4	5.5
136.7	4.85	140.0	5.51	0.31	5.6	6.5
141.0	4.63	144.0	5.30	0.27	5.1	6.1
145.3	4.68	148.0	5.41	0.31	5.7	6.6
148.5	5.22	151.0	6.07	0.33	5.5	6.5
153.7	6.01	155.8	7.04	0.39	5.5	6.5
		$E_{lab}=21.6\pm0.1$ MeV				
21.9	597	23.7	514	±18	3.4	5.3
24.6	484	26.7	418	15	3.5	5.3
32.6	259	35.2	226	8	3.7	5.5
37.0	159	39.9	140	5	3.6	5.4
42.1	82.4	45.3	73.1	3.0	4.1	5.7
46.6	47.0	50.0	42.0	1.3	3.0	4.7
50.6	28.4	54.3	25.7	0.8	3.2	4.7
53.4	20.8	57.3	18.9	0.7	3.5	4.9
56.2	18.9	60.2	17.2	0.5	3.1	4.7
59.6	18.3	63.8	16.8	0.6	3.6	5.0
63.0	19.4	67.3	18.0	0.6	3.4	4.8
66.6	20.6	71.0	19.4	0.7	3.4	4.9
70.6	21.0	75.1	19.9	0.7	3.4	4.9
75.6	21.4	80.3	20.6	0.7	3.3	4.8
80.3	20.6	85.0	20.1	0.7	3.3	4.8
85.3	18.4	90.1	18.2	0.6	3.4	4.9
90.2	15.8	95.0	15.8	0.8	4.7	6.2
95.5	12.4	100.3	12.6	0.5	4.0	5.2
100.3	9.34	105.1	9.66	0.36	3.7	5.0
105.6	7.24	110.2	7.60	0.30	3.9	5.2
110.7	6.17	115.2	6.58	0.27	4.1	5.3
115.9	5.10	120.2	5.51	0.24	4.3	5.5
120.9	5.28	125.1	5.78	0.25	4.3	5.5
126.3	5.34	130.2	5.93	0.26	4.4	5.5
131.7	5.54	135.3	6.22	0.27	4.3	5.5
137.1	6.02	140.3	6.85	0.29	4.2	5.4
142.4	6.45	145.3	7.41	0.30	4.0	5.2
147.6	6.98	150.2	8.10	0.33	4.1	5.3
156.0	8.20	158.0	9.63	0.39	4.0	5.2
		$E_{lab}=24.1\pm0.2$ MeV				
15.4	829	16.7	710	±26	3.6	5.6
24.7	518	26.7	447	15	3.4	4.8
29.6	346	32.0	301	12	3.9	5.7
36.9	158	39.8	139	6	4.1	5.3
41.8	84.8	45.0	75.1	2.9	3.8	5.7
46.5	39.7	50.0	35.5	1.3	3.5	4.9
51.1	21.9	54.8	19.8	0.7	3.6	4.9
53.2	19.0	57.1	17.2	0.8	4.3	5.4
56.0	16.8	60.0	15.3	0.6	3.8	5.1
58.9	16.3	63.0	15.0	0.6	3.8	5.1
62.7	18.2	67.0	16.9	0.7	4.0	5.2
65.6	18.6	70.0	17.4	0.7	4.2	5.8
70.5	19.9	75.0	18.9	0.7	3.6	4.9
75.3	19.1	80.0	18.3	0.7	3.6	5.0
80.3	18.1	85.0	17.7	0.6	3.4	5.2
86.0	15.5	90.8	15.4	0.6	3.7	5.0
89.9	12.6	94.7	12.6	0.6	4.7	5.8
95.2	9.17	100.0	9.24	0.34	3.7	5.0
100.3	6.61	105.0	6.84	0.27	4.0	5.2
105.3	4.77	110.0	5.01	0.23	4.7	5.8
110.5	3.53	115.0	3.76	0.18	4.8	5.8
115.7	2.66	120.0	2.87	0.12	4.3	5.5
120.9	1.92	125.0	2.10	0.09	4.2	5.4
129.5	1.38	133.2	1.55	0.08	5.3	6.3
136.5	1.022	139.8	1.161	0.070	6.0	6.9
142.0	0.998	145.0	1.146	0.049	4.3	5.4
150.6	0.780	153.0	0.909	0.044	4.8	5.9
		$E_{lab}=26.1\pm0.1$ MeV				
18.5	815	20.0	700	±35	5.0	6.4
27.8	371	30.0	321	12	3.6	5.1
32.4	236	35.0	206	7	3.4	5.3
36.9	142	39.8	125	5	3.7	5.4
41.8	72.3	45.0	64.0	2.4	3.7	5.2
46.5	36.6	50.0	32.8	1.2	3.8	5.5
50.3	26.0	54.0	23.5	1.0	4.1	5.7
53.2	19.8	57.0	18.0	0.8	4.3	5.9
56.0	18.2	60.0	16.6	0.5	3.0	4.6
59.4	16.9	63.5	15.6	0.6	3.7	5.1
62.7	18.1	67.0	16.8	0.6	3.6	5.0
66.6	18.2	71.0	17.0	0.5	2.9	4.5
70.5	17.6	75.0	16.7	0.6	3.6	5.0
75.3	15.8	80.0	15.2	0.4	2.5	4.3
80.3	13.2	85.0	12.9	0.4	3.1	4.7
85.2	11.5	90.0	11.4	0.4	3.2	4.7
90.2	9.50	95.0	9.54	0.37	3.9	5.1
95.2	7.17	100.0	7.31	0.28	3.9	5.1
100.3	5.35	105.0	5.53	0.23	4.2	5.4
105.4	4.25	110.0	4.46	0.18	4.2	5.2
110.5	3.18	115.0	3.38	0.13	3.8	5.0
115.7	2.66	120.0	2.87	0.12	4.3	5.5
120.9	2.13	125.0	2.33	0.10	4.1	5.3
126.1	1.68	130.0	1.86	0.08	4.1	5.3
131.4	1.73	135.0	1.95	0.08	4.1	5.3
136.7	1.72	140.0	1.95	0.08	4.1	5.3
142.0	1.76	145.0	2.02	0.08	4.1	5.3
147.4	1.74	150.0	2.02	0.08	4.2	5.4
150.0	1.72	152.4	2.01	0.08	4.2	5.4
156.0	1.61	157.9	1.89	0.08	4.2	5.4
		$E_{lab}=27.8\pm0.1$ MeV				
10.3	1368	11.1	1167	±39	3.4	5.2
13.9	1069	15.0	914	33	3.6	5.3
18.5	851	20.0	730	27	3.6	5.3
27.8	418	30.0	362	12	3.3	4.7
32.4	246	35.0	214	7	3.2	4.7
37.1	134.6	40.0	118.4	2.5	2.1	3.5
41.8	66.6	45.0	59.0	1.1	1.8	3.4
46.5	33.0	50.0	29.6	0.8	2.8	4.0
49.4	24.6	53.0	22.1	0.5	2.5	3.7
52.2	19.5	56.0	17.6	0.5	2.8	4.0
55.1	18.3	59.0	16.8	0.3	1.6	3.4
57.5	17.4	61.5	15.9	0.7	4.4	5.5
60.8	19.0	65.0	17.6	0.6	3.5	4.9
65.6	20.4	70.0	19.1	0.7	3.6	4.9
70.5	19.2	75.0	18.3	0.6	3.5	4.9
75.3	16.6	80.0	15.9	0.6	3.8	4.7
85.2	10.59	90.0	10.47	0.40	3.8	5.1
95.3	6.05	100.1	6.16	0.25	4.1	5.3
103.3	3.59	108.0	3.74	0.16	4.3	5.4
110.5	2.36	115.0	2.51	0.11	4.5	5.6
119.1	1.82	123.3	1.98	0.09	4.3	5.5
127.1	1.49	130.9	1.66	0.07	4.4	5.5
129.3	1.85	133.1	2.07	0.10	4.9	5.9
135.4	1.99	138.8	2.25	0.11	4.8	5.8
143.0	2.07	145.9	2.38	0.11	4.7	5.8
148.5	2.23	151.0	2.58	0.12	4.6	5.7
152.4	1.99	154.6	2.33	0.10	4.1	5.3
155.4	1.59	157.4	1.87	0.09	4.8	5.9

Figures 4, 5, 6, and 7 show the results of the measurements at 46.7°, 60.6°, 135.0°, and 145.0°, respectively. The data from the fixed-energy differential cross-section curves for 20.0 MeV$\leqslant E_p \leqslant$31.1 MeV, and the data of R. W. Peelle[4] and of W. Daehnick and R. Sherr[8] for 17.6 MeV$\leqslant E_p \leqslant$19.4 MeV, have been included for comparison. All differential cross-section-versus-energy data are tabulated in Table III. The measurements at 46.7° and 60.6° were relative and were normalized to the fixed-energy data. The good agreement of the present measurements with previously obtained values indicates the reliability of these data.

The variation of the elastic scattering cross section with the energy of the incident protons was first reported for this energy range by B. B. Kinsey.[12] The

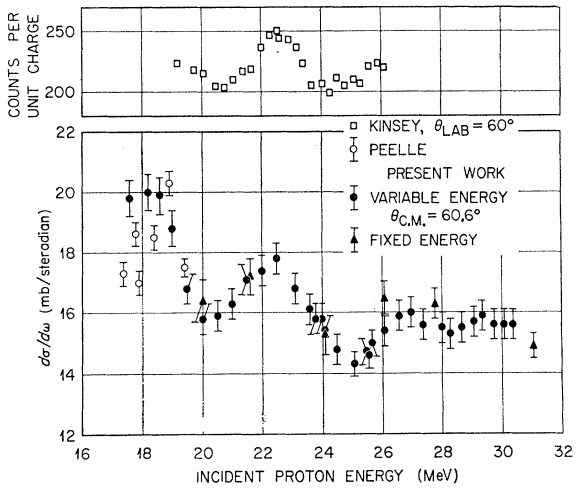

FIG. 5. Differential elastic scattering cross sections at $\theta_{c.m.}=60.6°$. The data labeled "Peelle" were taken from Ref. 4 and those labeled "Kinsey" were taken from Ref. 12.

energy dependence of the differential cross section near the first minimum was investigated, and a resonance at ~22.5 MeV was reported. These data are compared to the present work in Fig. 5. The variation in cross section near the second minimum is much more pronounced (see Figs. 6 and 7). The analysis of these data using the diffuse surface optical model is nearly complete and early publication of these results is planned.[13] Preliminary results[14] show that the over-all variation from 20 to 31 MeV can be reproduced by changing from surface to volume absorption.

B. Inelastic Scattering

(i) 4.4-MeV Level

The measured differential cross sections and associated errors for protons inelastically scattered from the

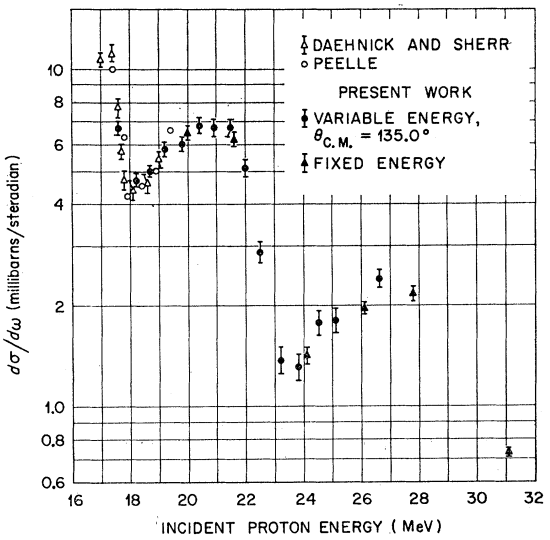

FIG. 6. Differential elastic scattering cross sections at $\theta_{c.m.}=135°$. The data labeled "Peelle" were taken from Ref. 4 and those labeled "Daehnick and Sherr" were taken from Ref. 8.

2^+ 4.4-MeV level of C^{12} are presented in Fig. 8.[15] The angular distributions are strongly peaked forward, and there is a definite change in the shapes of the curves as the incident energy is varied. The energy dependence is not as pronounced as for the elastic distributions. Figures 9 and 10 illustrate data taken at $\theta_{c.m.}\sim$135 and 145 deg.[15]

The asymmetry of the experimental data suggests

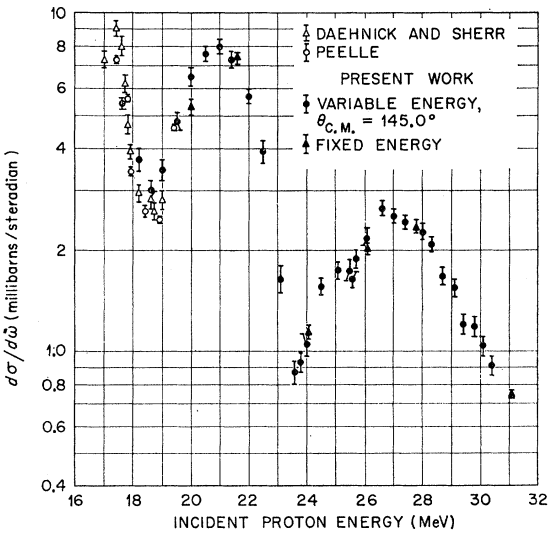

FIG. 7. Differential elastic scattering cross sections at $\theta_{c.m.}=145°$. The data labeled "Peelle" were taken from Ref. 4 and those labeled "Daehnick and Sherr" were taken from Ref. 8.

[12] B. B. Kinsey, Phys. Rev. **99**, 332 (1955).
[13] M. A. Melkanoff, J. S. Nodvik, C. N. Waddell, and J. K. Dickens (unpublished).
[14] J. K. Dickens, D. A. Haner, and C. N. Waddell, Bull. Am. Phys. Soc. **7**, 285 (1962).
[15] These differential cross sections are reported in tabular form in the Ph.D. dissertation of J. K. Dickens, University of Southern California, 1962, Order No. 63-2146 (University Microfilms, Inc., Ann Arbor, Michigan).

TABLE III. Differential cross sections for the elastic scattering of protons by C^{12} for various energies at four angles.

E_{lab} (MeV)	$(d\sigma/d\omega)_{c.m.}$ (mb/sr)	Relative % error	Absolute % error
	$\theta_{c.m.}=46.7°$		
17.6	77.4	3.0	6.0
18.2	78.0	3.0	6.0
18.7	74.2	3.0	6.0
19.2	69.8	3.0	6.0
19.8	64.3	4.0	6.0
20.4	60.6	4.0	6.0
20.9	61.4	4.0	6.0
21.5	61.4	4.0	6.0
22.0	61.6	4.0	6.0
22.5	61.1	4.0	6.0
23.2	60.8	4.0	6.0
23.8	57.9	4.0	6.0
24.5	55.2	4.0	6.0
25.1	54.9	4.0	6.0
	$\theta_{c.m.}=60.6°$		
17.6	20.5	4.0	5.0
18.2	20.7	4.0	5.0
18.6	20.6	4.0	5.0
19.0	19.4	4.0	5.0
19.5	17.4	4.0	5.0
20.0	16.3	4.0	5.0
20.5	16.4	4.0	5.0
21.0	16.8	4.0	5.0
21.5	17.7	4.0	5.0
22.0	18.0	4.0	5.0
22.5	18.4	4.0	5.0
23.1	17.4	3.0	5.0
23.6	16.7	3.0	5.0
23.8	16.3	3.0	5.0
24.0	16.3	3.0	5.0
24.1	15.9	3.0	5.0
24.5	15.3	3.5	5.0
25.1	14.8	3.5	5.0
25.5	15.2	3.5	5.0
25.6	15.1	3.5	5.0
25.7	15.5	3.5	5.0
26.1	15.9	3.5	5.0
26.6	16.4	3.5	5.0
27.0	16.5	3.0	5.0
27.4	16.1	3.0	5.0
28.0	16.0	3.0	5.0
28.3	15.8	3.0	5.0
28.7	16.0	3.0	5.0
29.1	16.2	3.0	5.0
29.4	16.4	3.0	5.0
29.8	16.1	3.0	5.0
30.1	16.1	3.0	5.0
30.4	16.1	3.0	5.0

E_{lab} (MeV)	$(d\sigma/d\omega)_{c.m.}$ (mb/sr)	Relative % error	Absolute % error
	$\theta_{c.m.}=135.0°$		
17.6	6.72	4.2	5.8
18.2	4.66	4.7	6.2
18.7	5.03	4.6	6.1
19.2	5.75	4.4	5.9
19.8	6.04	5.4	6.7
20.4	6.77	5.2	6.5
20.9	6.67	5.2	6.5
21.5	6.73	5.2	6.5
22.0	5.08	5.7	7.0
22.5	2.88	7.1	8.2
23.2	1.37	9.8	10.6
23.8	1.31	8.9	9.7
24.5	1.78	8.4	9.3
25.1	1.80	8.7	9.6
26.6	2.39	5.9	7.2
	$\theta_{c.m.}=145.0°$		
17.6	5.35	4.6	6.1
18.2	3.66	7.3	8.3
18.6	3.04	7.5	8.5
19.0	3.44	6.8	7.9
19.5	4.82	5.9	7.2
20.0	6.47	5.3	6.7
20.5	7.57	5.1	6.5
21.0	8.02	5.0	6.4
21.4	7.31	5.1	6.5
21.5	7.19	5.2	6.5
22.0	5.74	5.6	6.9
22.5	3.91	6.4	7.6
23.1	1.65	9.1	9.8
23.6	0.87	7.6	8.6
23.8	0.93	6.5	7.7
24.0	1.05	7.9	8.9
24.1	1.16	4.3	5.8
24.5	1.57	6.0	7.2
25.1	1.74	5.8	7.0
25.5	1.74	6.7	7.8
25.6	1.64	5.3	6.7
25.7	1.89	6.5	7.6
26.1	2.19	6.1	7.3
26.6	2.66	5.3	6.6
27.0	2.52	4.6	6.1
27.4	2.42	4.7	6.2
28.0	2.27	5.3	6.6
28.3	2.08	5.4	6.7
28.7	1.67	5.9	7.1
29.1	1.55	6.0	7.2
29.4	1.21	6.6	7.7
29.8	1.19	6.6	7.8
30.1	1.04	6.3	7.5
30.4	0.91	6.6	7.7

the presence of a direct interaction mechanism and invites comparison with direct reaction theory. In the distorted-wave Born approximation (DWBA),[16] the scattering amplitude between an initial channel i and a final channel f is given by

$$f_{fi}(\mathbf{k}_f,\mathbf{k}_i)\simeq(k_f/k_i)^{1/2}(\mu/2\pi\hbar^2)\int\psi_f^{(-)}(\mathbf{r})^*\times V_{fi}(\mathbf{r})\psi_i(\mathbf{r})d\mathbf{r}. \quad (1)$$

[16] C. A. Levinson and M. K. Banerjee, Ann. Phys. (N. Y.) 2, 471 (1957). C. A. Levinson, in *Nuclear Spectroscopy*, edited by F. Ajzenberg-Selove (Academic Press, Inc., New York, 1960), Part B, p. 670. W. Tobocman, *Theory of Direct Nuclear Reactions* (Oxford University Press, London, 1961).

V_{fi}, the matrix element of the interaction potential V, is

$$V_{fi}=\int\phi_f(\xi)^*V\phi_i(\xi)d\xi, \quad (2)$$

where $\phi_f(\xi)$ and $\phi_i(\xi)$ are target eigenfunctions, and the variables ξ include positions, spins, and isotopic spins. The wave functions $\psi_i(\mathbf{r})$ and $\psi_f^{(-)}(\mathbf{r})$ describe the relative motions of the scattering nucleon and the target. At large distances $\psi_i(\mathbf{r})$ consists of a plane wave in the direction of $\mathbf{k}_i$ plus outgoing spherical waves and $\psi_f^{(-)}(\mathbf{r})$ consists of a plane wave in the direction of $\mathbf{k}_f$ plus incoming spherical waves.

Simplification is obtained by assuming V as being of zero range and using plane waves for $\psi_i(\mathbf{r})$ and $\psi_f^{(-)}(\mathbf{r})$. This simplification leads to the result

$$d\sigma/d\omega = (k_f/k_i)\Sigma_l A_l |(u_f|\, j_l(Qr)\,|u_i)|^2, \qquad (3)$$

where $\mathbf{Q}=\mathbf{k}_f-\mathbf{k}_i$. The u_f and u_i are radial wave functions of the struck target particle, evaluated at the position of the incident particle. The sum over l is restricted by various selection rules. The A_l are constants which depend on the target structure.

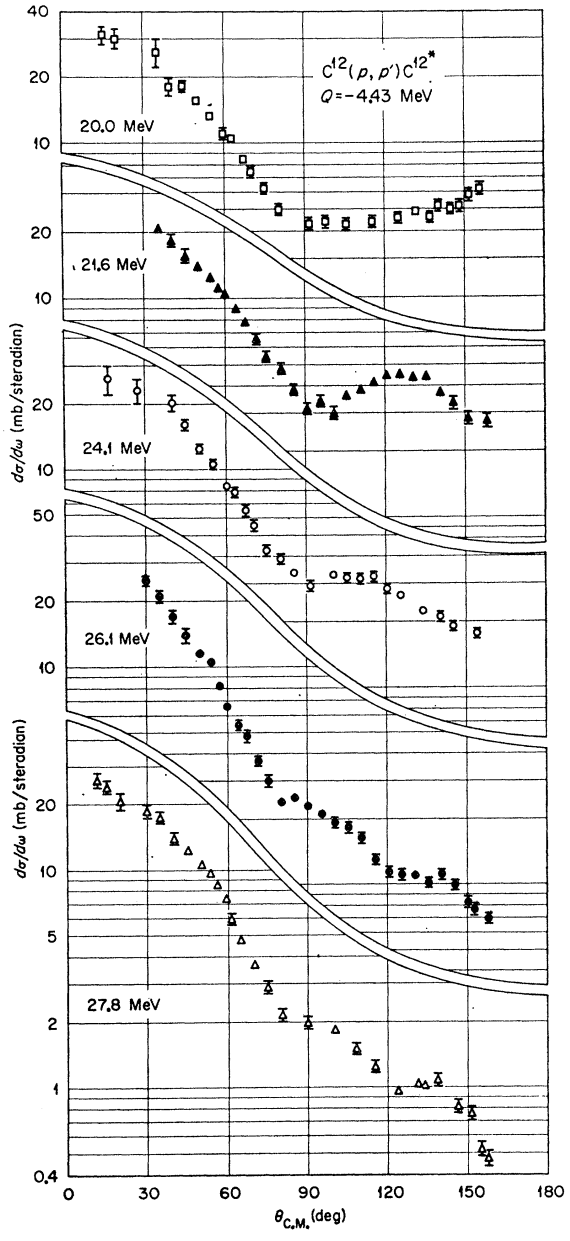

FIG. 8. Five angular distributions of protons inelastically scattered from the 4.43-MeV level of C^{12}.

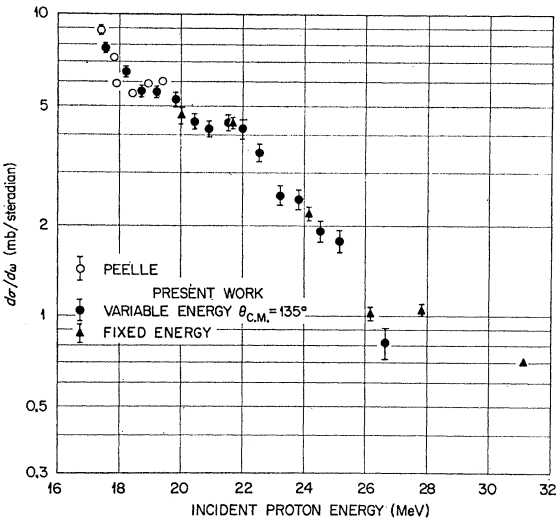

FIG. 9. Differential cross sections for protons inelastically scattered from the 4.43-MeV level of C^{12} at $\theta_{c.m.}\approx 135.4°$. The data labeled "Peelle" were taken from Ref. 4.

Figure 11 illustrates the present experimental differential cross sections for scattering by the 4.4 MeV level and includes curves representing this inelastic scattering previously reported.[2,4,17] The abscissa in Fig. 11 is the momentum transfer (in units of $\hbar\times 10^{13}$/cm) and the ordinate is $(k_i/k_f)(d\sigma(\theta)/d\omega)$. The zero-range, plane-wave Born approximation theory, Eq. (3), predicts that these angular distributions should coincide.

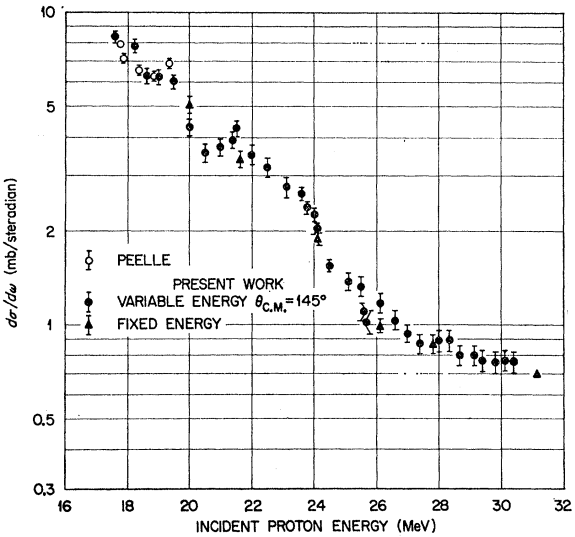

FIG. 10. Differential cross sections for protons inelastically scattered from the 4.43-MeV level of C^{12} at $\theta_{c.m.}\approx 145.4°$. The data labeled "Peelle" were taken from Ref. 4.

[17] S. W. Chen and N. M. Hintz, University of Minnesota Linear Accelerator Progress Report, 1958 (unpublished). K. Strauch and F. Titus, Phys. Rev. **103**, 200 (1956). H. Tyrén and T. A. J. Maris, Nucl. Phys. **3**, 52 (1957).

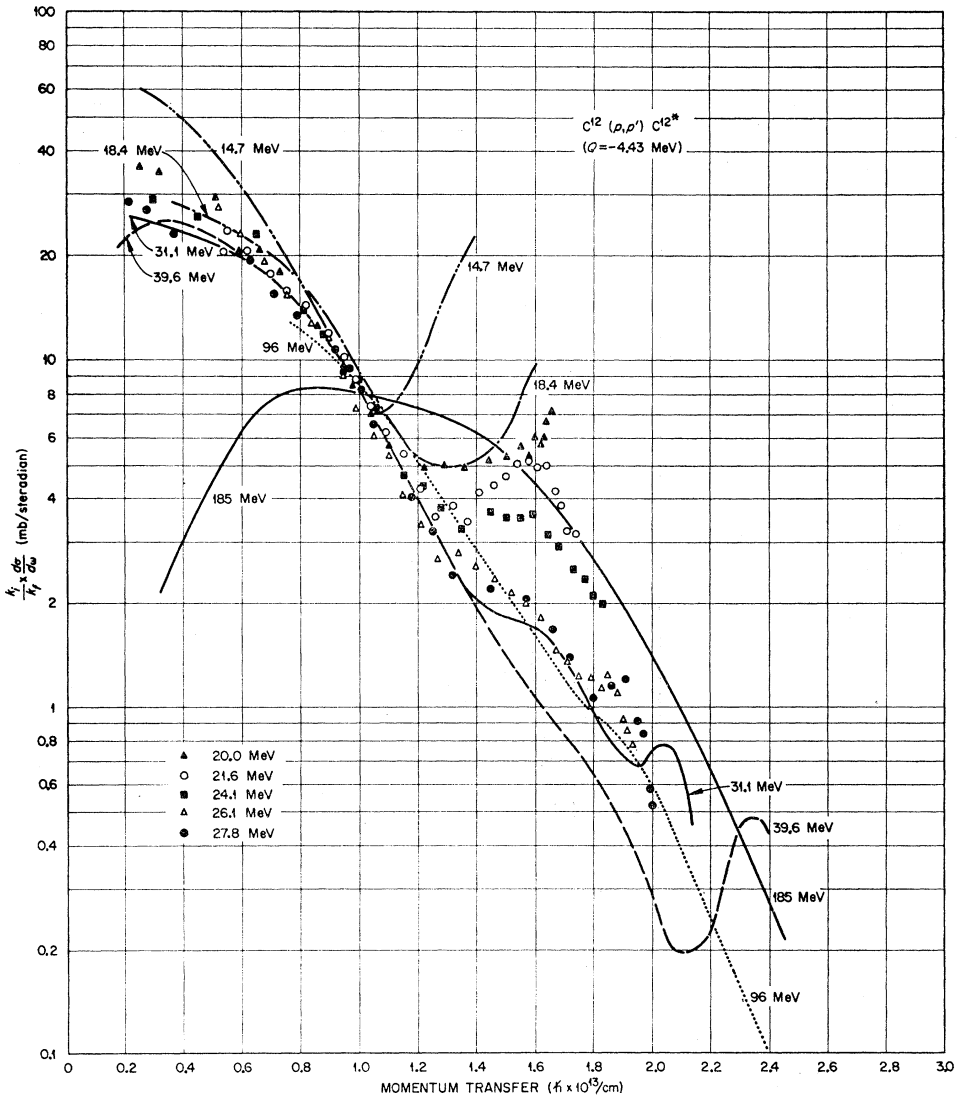

FIG. 11. Differential cross sections for protons inelastically scattered from the 4.43-MeV level of C^{12}. The abscissa is momentum transfer, $|\mathbf{k}_f-\mathbf{k}_i|$ in units of $\hbar\times10^{13}$/cm. The solid curves represent angular distributions previously obtained and reported in Refs. 2, 4, and 17.

In addition, this approximation predicts very small differential cross sections in the forward direction. Both predictions are contrary to experiment implying that the approximations of plane waves and zero range are not valid for carbon.

Using the more exact DWBA theory, Eq. (1), requires considerable numerical calculation. The distorted waves $\psi_i(\mathbf{r})$ and $\psi_f^{(-)}(\mathbf{r})$ are obtained by solving optical-model equations using a nuclear optical potential which best reproduces elastic scattering data. Levinson and Banerjee[18] have analyzed scattering of protons by the 4.4-MeV level using the DWBA theory. A series of fits to inelastic data for 14 MeV$\leqslant E_p\leqslant$185 MeV were obtained. Their analysis showed that the distorted-wave formalism is capable of reproducing correct dependence of the inelastic scattering amplitudes on energy and scattering angle. Nevertheless, several points (including the large interaction strength which must be used to give the required large cross sections[19]) remain to be clarified.

(*ii*) 7.7-MeV Level

Differential cross sections for scattering by the 0^+ state at 7.7-MeV are shown in Fig. 12.[15] Features of scattering by this level are (a) forward peaking, (b) small differential cross sections, (c) a definite diffraction pattern, (d) relative energy independence of the shape of the curve, and (e) a shift of the second minimum toward larger angles with increasing energy. The zero-range, plane-wave Born approximation predicts a shift in the opposite direction for fixed interaction radius.

[18] C. A. Levinson and M. K. Banerjee, Ann. Phys. (N. Y.) 3, 67 (1958).

[19] N. Austern, in *Fast Neutron Physics*, edited by J. B. Marion and J. L. Fowler (Interscience Publishers, Inc., New York, 1963), Vol. 2, Chap. VD.

(iii) 9.6-MeV Level

Differential cross sections for scattering by the (3^-) state at 9.6-MeV are shown in Fig. 13.[15] Features of scattering by this level are (a) broad forward peaking, (b) energy independence of the shape of the curve, and (c) a gradual decrease in differential cross sections with increasing energy. These angular distributions are very similar to those reported at lower energies[4] and at 31 MeV.[2]

(iv) 12.7-MeV Level

Differential cross sections for the (1^+) state at 12.7-MeV at $E_p=27.8$ MeV are shown in Fig. 14.[15] A larger uncertainty in cross section was introduced for this level because the peak was superimposed on the proton continuum from the $C^{12}(p,p')3\alpha$ breakup. Because the counting errors for each point were large, the data for two or three angles were combined to reduce these errors.

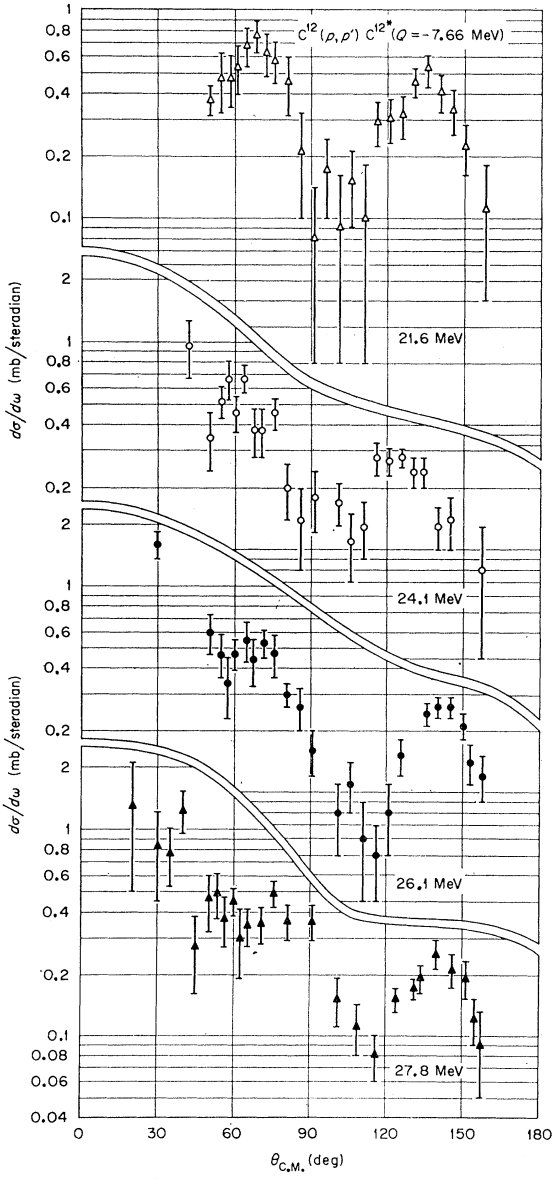

FIG. 12. Four angular distributions of protons inelastically scattered from the 7.66-MeV level of C^{12}.

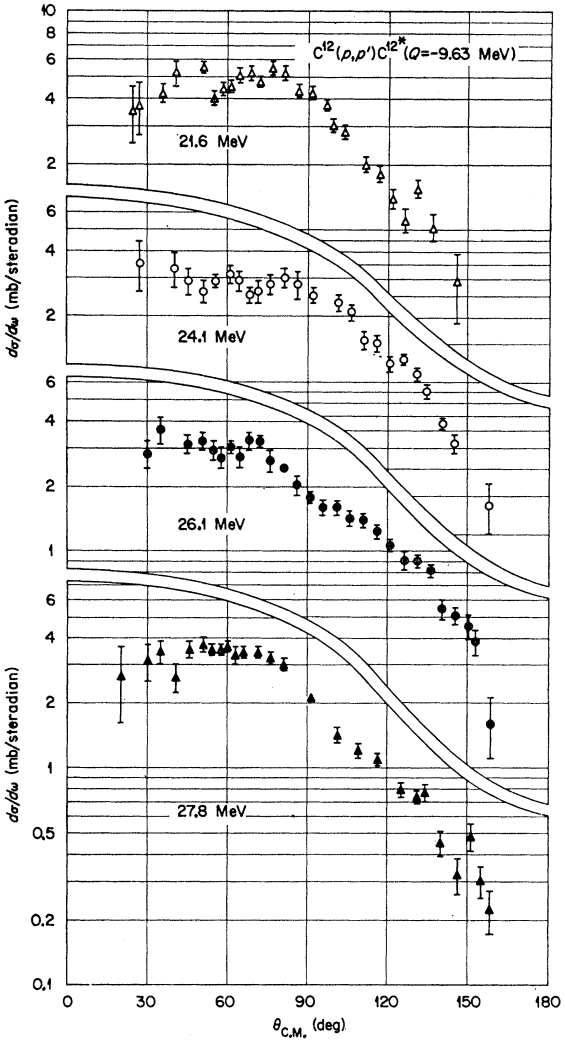

FIG. 13. Four angular distributions of protons inelastically scattered from the 9.63-MeV level of C^{12}.

(v) Integrated Partial Cross Sections

The integrated partial cross sections corresponding to the reported inelastic angular distributions are shown in Fig. 15.[15] The integrals were obtained after extrapolating the measurements to large and small angles, and the quoted errors include the estimated reliability of this extrapolation. For comparison the values of R. Peelle[4] and of E. Warburton and H. Funsten[20] are included.

[20] E. K. Warburton and H. O. Funsten, Phys. Rev. **128**, 1810 (1962).

V. SUMMARY

Elastic scattering of protons by C^{12} has been measured for incident proton energies between 18 and 30 MeV. Angular distributions and integrated partial cross sections for proton scattering leading to the excitation of the 4.4-, 7.7-, 9.6-, and 12.7-MeV levels in C^{12} are reported.

The dominant feature of elastic scattering is the strong energy dependence of the angular distribution. Inelastic scattering angular distributions do not exhibit this strong energy dependence. Angular distributions of inelastically scattered protons are peaked forward for all levels studied. The shape and energy dependence of the angular distribution of scattering by the 4.4-MeV level indicates that the zero-range, plane-wave Born approximation cannot be expected to reproduce these data.

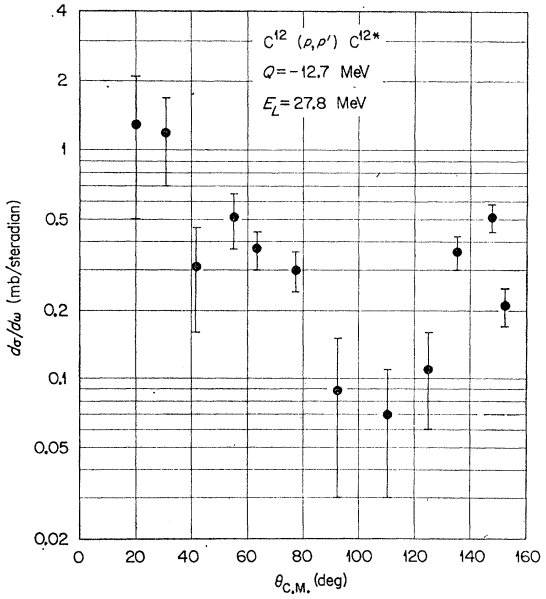

FIG. 14. The angular distribution of 27.8-MeV protons inelastically scattered from the 12.7-MeV level of C^{12}.

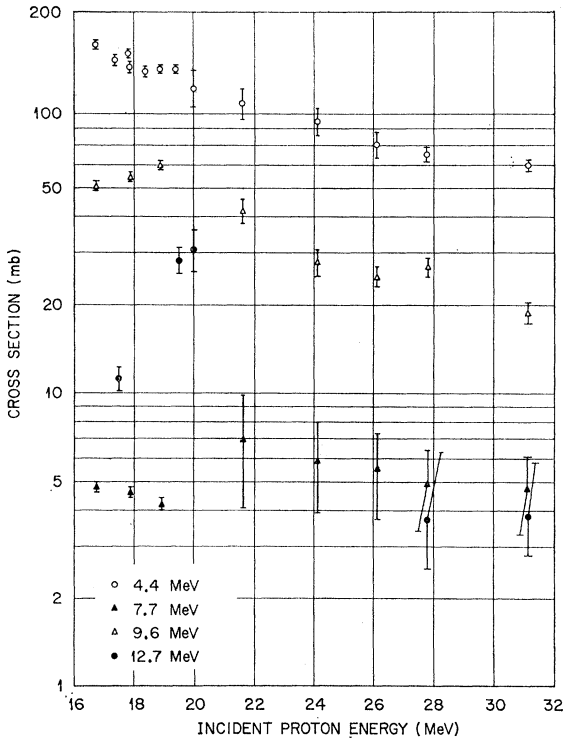

FIG. 15. Integrated partial cross sections for protons inelastically scattered from the 4.43-, 7.66-, 9.63-, and 12.7-MeV levels of C^{12}. The data at $E_p \leqslant 19.4$ MeV for protons inelastically scattered from the 4.43-, 7.66-, and 9.63-MeV levels were taken from Ref. 4. The data at $E_p \leqslant 20$ MeV for protons scattered from the 12.7-MeV level were taken from Ref. 20. The data at $E_p = 31.1$ MeV were taken from Ref. 2.

ACKNOWLEDGMENTS

We gratefully acknowledge the generous assistance of J. Sirois and the crew of the University of Southern California Linear Accelerator. We wish to thank Dr. J. Nodvik for his continuing interest and many helpful comments.